Two Conformational Changes Are Associated with Glutamate Translocation by the Glutamate Transporter EAAC1†

Carsten Mim,‡,§ Zhen Tao,‡ and Christof Grewer*,‡

Department of Physiology, University of Miami School of Medicine, 1600 NW 10th Avenue, Miami, Florida 33136, and Max-Planck-Institute for Biophysics, Max-von-Laue-Strasse 3, D-60438 Frankfurt, Germany

Received March 20, 2007; Revised Manuscript Received May 30, 2007

ABSTRACT: Glutamate is transported across membranes by means of a carrier mechanism that is thought to require conformational changes of the transport protein. In this work, we have determined the thermodynamic parameters of glutamate and the Na^+ binding steps to their extracellular binding sites along with the activation parameters of rapid, glutamate-induced processes in the transport cycle by analyzing the temperature dependence of glutamate transport at steady state and pre-steady state. Our results suggest that glutamate binding to the transporter is driven by a negative reaction enthalpy ($\Delta H^0 = -33$ kJ/mol), whereas the tighter binding of the non-transportable inhibitor TBOA is caused by an additional increase in entropy. Processes linked to the binding of glutamate and Na^+ to the transporter are associated with low activation barriers, indicative of diffusion-controlled reactions. The activation enthalpies of two processes in the glutamate translocation branch of the transport cycle were $\Delta H^‡ = 95$ kJ/mol and $\Delta H^‡ = 120$ kJ/mol, respectively. Such large values of $\Delta H^‡$ suggest that these processes are rate-limited by conformational changes of the transporter. We also found a large activation barrier for steady-state glutamate transport, which is rate-limited by the K^+-dependent relocation of the empty transporter. Together, these results suggest that two conformational changes accompany glutamate translocation and at least one conformational change accompanies the relocation of the empty transporter. We interpret the data with an alternating access model that includes the closing and opening of an extracellular and an intracellular gate, respectively, in analogy to a hypothetical model proposed previously on the basis of the crystal structure of the bacterial glutamate transporter GltPh.

Glutamate transporters contribute to the removal of the neurotransmitter glutamate from the extracellular space after glutamatergic neurotransmission has taken place by transporting glutamate into neurons and glia cells surrounding the respective synaptic contact. It was shown in several reports that glutamate uptake can have a direct effect on the time dependence of glutamate receptor responses triggered by pre-synaptic release (*1*−*5*). It was proposed that the rapid buffering of glutamate by binding to its transporter binding sites (*6*) and glutamate translocation across the membrane in the millisecond time range (*1*, *7*, *8*) contribute to shaping the temporal profile of the glutamate concentration in the synapse. However, up until now the rates of the glutamate binding reaction and the steps associated with translocation have been determined only at room temperature. It is unknown how the rates of these reaction steps change when the temperature is elevated to physiological levels.

Active transport processes are known to be strongly affected by temperature. Consistently, the steady-state turnover of the glutamate transporter subtype excitatory amino acid transporter 1 (EAAT[1]1) was shown to be accelerated by increasing temperature with a Q_{10} value of 3.2, as determined by transport current recording from EAAT1-expressing *Xenopus* oocytes (*9*). This result suggested that steady-state turnover is associated with conformational changes of the transporter. It was proposed that the K^+-dependent relocation of the transporter, which occurs independently from the glutamate translocation step (*10*), is rate-limiting for glutamate transport at room temperature (*7*, *8*). Therefore, the temperature dependence of the glutamate transport rate at steady state most likely reflects the temperature dependence of this transporter relocation reaction. The temperature dependencies of other partial reaction steps in the transport cycle, such as glutamate binding and glutamate translocation, have not been determined previously. Knowledge of the temperature dependencies of these steps allows one to separate the enthalpic from the entropic contributions to the free energies of activation of these partial reactions (*11*).

In this work, we determined the temperature dependence of the steady-state kinetics and the pre-steady-state kinetics

† This work was supported by grants from the National Institutes of Health (R01-NS049335-02) and the Deutsche Forschungsgemeinschaft (GR 1393/2-2,3) awarded to C.G. Z.T. is grateful for an American Heart Association postdoctoral fellowship.

* Corresponding author. Phone: (305) 243-1021. Fax: (305) 243-5931. E-mail: cgrewer@med.miami.edu.

‡ University of Miami School of Medicine.

§ Max-Planck-Institute for Biophysics.

[1] Abbreviations: EAAC1, excitatory amino acid carrier 1; EAAT, excitatory amino acid transporter; GltPh, glutamate/aspartate transporter from *Pyrococcus horikoshii;* TBOA, DL-*threo*-β-benzyloxyaspartate; EGTA, ethylene glycol-bis(2-aminoethylether)-*N*,*N*,*N*′,*N*′-tetraacetic acid; HEK, human embryonic kidney; HEPES, 4-(2-hydroxyethyl)-piperazine-1-ethanesulfonic acid; Mes, methanesulfonate; MNI, 4-methoxy-7-nitroindolinyl; NMG^+, *N*-methylglucamine$^+$; SLC, solute carrier.

10.1021/bi7005465 CCC: $37.00
Published on Web 07/13/2007

of substrate transport by the neuronal glutamate transporter EAAC1 (excitatory amino acid carrier 1), in order to obtain insight into the diffusional processes/conformational changes that were proposed to accompany glutamate transport. The main findings of this study are as follows: (1) Substrate binding to EAAC1 is driven thermodynamically by a negative binding enthalpy and, for a competitive inhibitor, an increase in entropy, and is kinetically associated with a low-energy barrier (diffusion controlled). (2) Na^+ binding to EAAC1 in the absence of amino acid substrate is isenthalpic and driven thermodynamically by an increase in entropy. (3) Two processes in the glutamate-dependent half-cycle of EAAC1 possess high activation barriers, suggesting that conformational changes accompany glutamate translocation. (4) The kinetics of activation by the substrate and the inactivation of anion currents show the same temperature dependence as that of two of the three pre-steady-state components of the electrogenic transport current. On the basis of these findings, we propose that two conformational changes take place in the glutamate-dependent half-cycle of EAAC1. On the basis of a structural model reported by Yernool and colleagues (*12*), we propose that these conformational changes are glutamate-induced closing of an extracellular gate and the subsequent opening of an intracellular gate, allowing glutamate dissociation into the cytoplasm. The EAAC1-associated anion current is modulated as the transporter transitions between these different conformations.

MATERIALS AND METHODS

Cell Culture and Transfection. HEK293 cells (American Type Culture Collection No. CRL 1573) were cultured as described previously (*7*, *13*). The cell cultures were transiently transfected with EAAC1 cDNA inserted into a pBK-CMV-expression plasmid by using FuGene transfection reagent according to the protocol supplied by the manufacturer (Roche, Basel, Switzerland). One day after transfection, the cells were used for electrophysiological measurements.

Whole-Cell Current Recording. Glutamate-induced and Na^+-induced EAAC1 currents were measured in the whole-cell current recording configuration (*14*). Whole-cell currents were recorded with an EPC7 patch-clamp Amplifier (ALA Scientific, Westbury, NY) under voltage-clamp conditions. The resistance of the recording electrode was 2−3 MΩ. As described previously (*7*), intracellular SCN^- was used in some recordings to enhance glutamate-induced EAAC1 anion currents. The direction of the SCN^- concentration gradient across the membrane was controlled by the composition of the internal and external solutions containing 130 mM KSCN, 1 mM $MgCl_2$, 10 mM EGTA, and 10 mM HEPES (pH 7.3), or 140 mM NaCl, 2 mM $MgCl_2$, 2 mM $CaCl_2$, and 10 mM HEPES (pH 7.3) for SCN^- outflow, respectively. SCN^- inflow was generated by the substitution of external NaCl with NaSCN, and the pipet solution contained KCl instead of KSCN. Transport currents caused by electrogenic glutamate movement across the membrane were studied after replacing extracellular and intracellular anions with impermeable methanesulfonate (Mes^-), thus eliminating any anion current component.

In the whole-cell recordings performed at steady state, series resistance was not compensated because of the small whole-cell currents carried by EAAC1. However, series resistance compensation of 60−80% was used in the whole-cell recording experiments involving step changes of the membrane potential in order to accelerate the capacitive charging of the membrane in response to the voltage jump. Typical time constants for membrane charging under these conditions were 200−250 μs.

Laser Photolysis of Caged Glutamate, Rapid Solution Exchange, and Temperature control. Laser-pulse photolysis experiments were performed as described previously (*15*), except that we used 4-methoxy-7-nitroindolinyl (MNI)-caged glutamate instead of α-carboxy-2-nitrobenzyl glutamate. Both caged compounds are inert with respect to the glutamate transporter EAAC1 (*7*, *16*). Briefly, MNI-caged glutamate (TOCRIS, Ellisville, MS) at concentrations of 500 μM to 2 mM was applied by means of a small quartz tube (350 μm diameter) to the cells with a velocity of 5 cm/s, resulting in an effective time resolution of the solution exchange of 20−30 ms (10−90% rise time with whole cells). Photolysis of caged glutamate was initiated with a light flash (340 nm, 15 ns, excimer laser pumped dye laser, Lambda Physik), which was delivered to the cell with an optical fiber (350 μm diameter). Laser energies were varied in the range of 50−450 mJ/cm^2 with neutral density filters. The instrument time constant of the photolysis/patch-clamp recording system was previously determined as ∼20 μs, by injection of a square current pulse into the I-V converter under typical whole-cell recording conditions (10 kHz Bessel filter, (*17*)). This instrument time constant is less than 1/10th of that of the fastest EAAC1 process observed in this work. To control the temperature of the solutions flowing over the EAAC1-expressing cells, the tubes delivering the solutions to the cell were suspended in a homemade water-jacketed device, which was held at a preset constant temperature using a circulating thermostat (VWR, West Chester, PA). The bath temperature in the measuring chamber for whole-cell recording was also adjusted to the same value as that of the out-flowing solutions by using the same circulating thermostat in order to prevent temperature gradients between the out-flowing solutions and the bath. We determined the temperature at the outlet of the quartz tube, where the voltage-clamped cells were positioned, with a micro-temperature probe (0.011 in. diameter, Physitemp, Clifton, NJ). Because of the 10-fold larger dead volume of the temperature-controlled solution exchange device, the effective time required for complete solution exchange around the cell surface was at least 10 times that of the device without temperature control. Most temperature-dependent experiments were performed at 0 mV transmembrane potential because of the optimal stability of the HEK293 cells at this potential and the ability to compare the data with previous results (*7*, *17*).

At any temperature, the release of glutamate by the photolytic reaction should be faster than the slowest step in the reaction cycle in order to prevent MNI-glutamate photolysis from limiting the rate of the observed transporter reaction. The rate of photolytic release of glutamate from MNI-glutamate is expected to be temperature dependent, slowing down at reduced temperatures. However, the temperature dependence of the photolysis rate of MNI-glutamate is not known. The following estimation suggests that the temperature dependence of MNI photolysis should not affect the activation parameters determined here for the glutamate

transport process. At room temperature, the time constant of the MNI-glutamate photolysis reaction is 200 ns (*18*), whereas the time constant of the fastest process in the EAAC1 transport cycle studied here is about 1000-fold larger (300 μs). If photolytic glutamate release would be rate limiting for the glutamate-induced current rise at 17 °C, which is the fastest process observed at this temperature (τ ~330 μs), then the time constant for photolysis would have to increase 1000-fold in this temperature interval (room temperature to 17 °C). The resulting activation energy would be ~830 kJ/mol. It is highly unlikely that the MNI-glutamate photolysis reaction is associated with such a high activation barrier for two reasons: (1) Organic reactions in solution typically have activation energies ranging from 40 to 120 kJ/mol, and activation energies much higher than that are unusual (*19*, *20*). (2) The activation energy of photolysis of caged ATP, which is not identical to and slower than that of MNI-glutamate on the basis of nitrobenzyl photochemistry, was determined as only 55 kJ/mol (*21*). Therefore, it is unlikely that the rate of glutamate release by photolysis limits the rate of the current rise, even at 17 °C, the lowest temperature used in this study.

The whole-cell currents were low-pass filtered at 1−20 kHz and recorded with pClamp8 software (Molecular Devices, Sunnyvale, CA). The experimental data were evaluated using Origin software (OriginLabs, Northampton, MA).

Evaluation of Temperature-Dependent Data. To estimate the effect of temperature on several key kinetic parameters, including glutamate-induced steady-state currents carried by EAAC1 and reaction rates, we calculated the ratio of each parameter at two different temperatures, T, according to the following equation:

$$Q_{10} = \left(\frac{X_1}{X_2}\right)^{\left(\frac{10}{T1-T2}\right)} \quad (1)$$

Here, X_1 represents the parameter under study (current or rate) at the lower temperature, T_1, and X_2 represents this parameter at the higher temperature, T_2. To evaluate the temperature dependence of apparent dissociation constants, K_m, we used the van't Hoff equation (*22*).

$$\ln(K_m) = \frac{\Delta H^0}{R}\frac{1}{T} + c \quad (2)$$

$\ln(K_m)$ was plotted versus $1/T$, and from the slope, we obtained the apparent reaction enthalpy ΔH^0. We then calculated the reaction entropy, ΔS^0, from ΔH^0 and the free energy ΔG^0 at room temperature (22 °C) with the following equations:

$$\Delta G^0 = RT\ln(K_m) \quad (3\,a)$$

$$\Delta S^0 = (\Delta H^0 - \Delta G^0)/T \quad (3\,b)$$

The relationship between the rate constant of a reaction and the temperature was described by using ‡Eyring transition state theory (*23*).

$$\ln(1/\tau) - \ln\left(\frac{k_B T}{h}\right) = \frac{\Delta S^{\ddagger}}{R} + \frac{-\Delta H^{\ddagger}}{R}\cdot\frac{1}{T} \quad (4)$$

Here, $1/\tau$ is the apparent relaxation rate constant associated with a specific phase of the transporter reaction, $\Delta H^{\ddagger}$ is the activation enthalpy, and $\Delta S^{\ddagger}$ is the activation entropy. The activation parameters were then determined by plotting $\ln(1/\tau) - \ln(k_B T/h)$ versus $1/T$. The slope of this plot yields $\Delta H^{\ddagger}$, and the intercept yields $\Delta S^{\ddagger}$. The constants k_B and h have their usual meaning.

The voltage (V) dependence of the voltage-jump-induced charge movement, Q, was described with a Boltzmann-like relationship (Q_{max} is the maximum charge movement, and Q_{offset} is the holding-potential-dependent offset of the charge movement),

$$Q = \frac{Q_{max}}{1 + \frac{K_{Na}^{\ 0}}{[Na^+]}\exp\left(\frac{-z_Q F V}{RT}\right)} + Q_{offset} \quad (5)$$

in which the midpoint potential, $V_{1/2}$, of the charge movement is defined as follows:

$$V_{1/2} = \frac{RT}{z_Q F}\ln\left(\frac{[Na^+]}{K_{Na}^0}\right) \quad (6)$$

Here, z_Q is the apparent valence of the moved charge, K_{Na}^0 is the dissociation constant for Na^+ from EAAC1 at 0 mV transmembrane potential, and F is the Faraday constant. The voltage dependence of the relaxation rate, $1/\tau$, of the voltage-jump-induced current is described as follows:

$$1/\tau = k_f^0 \exp\left(\frac{-z_Q F V}{2RT}\right) + k_b^0 \exp\left(\frac{z_Q F V}{2RT}\right) \quad (7)$$

In this equation, k_f^0 and k_b^0 are the rate constant for the forward and backward reactions at $V = 0$, respectively.

RESULTS

Temperature Dependence of EAAC1 Kinetic Properties at Steady State. We first determined the effect of temperature on the glutamate-induced transport current at steady state. When 100 μM glutamate (a saturating concentration at room temperature) was applied to HEK cells transfected with EAAC1, an inward steady-state transport current was evoked with an average amplitude of 54 ± 12 pA (n = 4, 24 °C). The effect of temperature on this glutamate-induced transport current was substantial, with a Q_{10} of 3.7 ± 0.4 (n = 4, Figure 1A and C, ■), which is consistent with previous results reported for EAAT1 expressed in *Xenopus* oocytes (Q_{10} = 3.2, (*9*)) and as expected for a secondary active transport process.

Next, we investigated the influence of the temperature on glutamate-induced EAAC1 anion currents at steady state by applying 100 μM glutamate to EAAC1-expressing cells in the presence of intracellular SCN^- ions (original data are shown in Figure 1B). It was shown previously that under these ionic conditions about 90% of the EAAC1-mediated current is carried by SCN^- (*24*). The resulting currents were plotted as a function of the inverse temperature, as shown in Figure 1C (●). Elevated temperatures resulted in a smaller increase of the anion current (Q_{10} = 1.9 ± 0.4, n = 4) as compared to the transport current. This Q_{10} value implies a small energy barrier for the glutamate-induced flow of anions

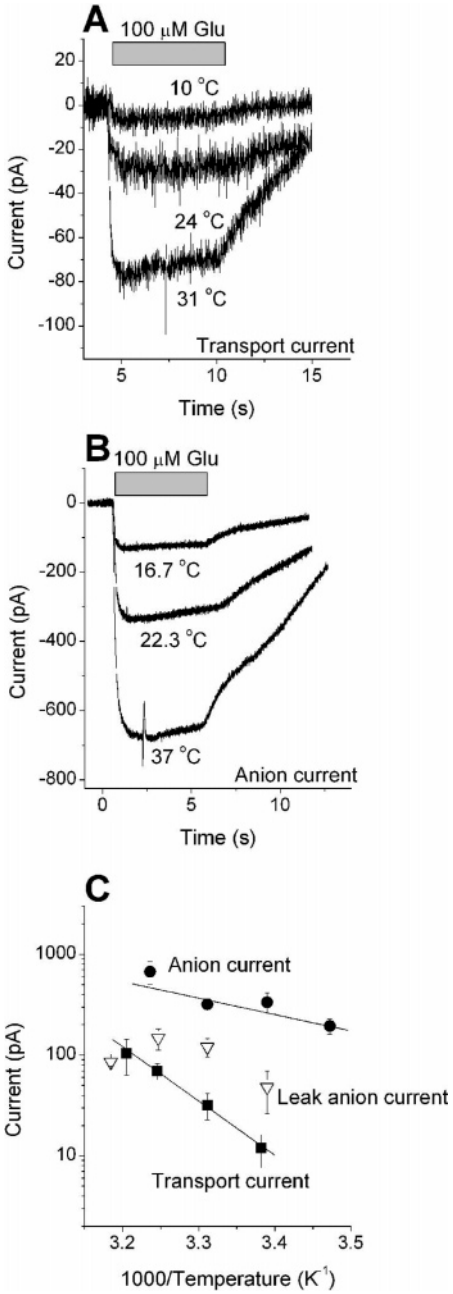

FIGURE 1: Steady-state glutamate transport is associated with a large activation barrier. (A) Typical transport currents recorded in response to the application of 100 μM glutamate to EAAC1 for the interval indicated by the gray bar at 10, 24, and 31 °C (0 mV transmembrane potential). The pipet contained 140 mM KMes. (B) Typical anion currents recorded in response to the application of 100 μM glutamate to EAAC1 for the interval indicated by the gray bar at 16.7, 22.3, and 37 °C (0 mV transmembrane potential). The pipet contained 140 mM KSCN. (C) Arrhenius plot of the three current components of EAAC1. The circles represent the glutamate-induced anion current (100 μM glutamate, internal KSCN). The triangles represent the leak anion current, which was induced by an application of 140 mM Na^+ to the transporter (internal KSCN). The squares represent the transport current (internal KMes). The lines are linear fits to the experimental data. The leak anion current was not fitted because of the significant scatter of the data.

across the membrane, which is expected for a diffusion-like process of anion movement through the transporter (*9*). Diffusion-controlled processes in aqueous solutions are typically associated with Q_{10} values of 1.3 to 1.6 (*25*).

In addition to the glutamate-activated anion conductance, EAAC1 catalyzes a leak anion conductance. This leak anion conductance is activated in the absence of glutamate by the binding of Na^+ to the empty transporter (*16*, *26*). To test the temperature dependence of the leak anion conductance, we recorded leak currents induced by the application of 140 mM Na^+ to EAAC1 in the presence of internal SCN^-. The resulting leak anion current generally increased with increasing temperature with a Q_{10} value of 1.7 ± 0.6 ($n = 6$, Figure 1C, ▽). This Q_{10} value for the leak anion current is as expected for a diffusion-limited process in water.

Effect of Temperature on the Apparent Substrate and Na^+ Dissociation Constants. To gain insight into the molecular processes involved in the association of the organic substrate and cations with the glutamate transporter, we first determined the temperature dependence of the apparent dissociation constant, K_m, of EAAC1 for glutamate by analyzing the [glutamate] dependence of the EAAC1 transport current. Under forward transport conditions (140 mM K^+ internal) and at room temperature (22 °C), the apparent K_m for glutamate was 10.3 ± 1.4 μM, consistent with previous reports (*7*, *15*). The temperature dependence of the K_m is shown in Figure 2C as a van't Hoff plot (eq 2, ■). This van't Hoff plot shows linear behavior, indicating that the apparent reaction enthalpy (ΔH^0) is constant within the chosen temperature interval. ΔH^0 was derived from the slope of the $\ln(K_m)$ versus $1/T$ relationship to be -33 ± 6 kJ/mol (Figures 2C and D). The apparent reaction entropy was calculated from eqs 3a and 3b to be $\Delta S^0 = -15 \pm 8$ J/K·mol (the thermodynamic parameters are also summarized in Table 1). These results indicate that enthalpic factors dominate the apparent ΔG^0 of glutamate association with EAAC1 at room temperature.

In a previous report, we showed that the apparent affinity for glutamate of the glutamate transporter subtype EAAT4 expressed in HEK cells is almost 10-fold higher than that of EAAC1 expressed in the same cell line (*13*), and its affinity is also much higher than those of the glutamate transporter subtypes EAAT1 and 2 (unpublished results). This is an interesting phenomenon because it indicates significant differences in the substrate binding environment between EAAT4 and EAATs 1−3. Therefore, we tested whether this higher substrate affinity of EAAT4 is accompanied by changes in the enthalpy/entropy contributions to the apparent K_m of EAAT4 for glutamate. The temperature dependence of the K_m of EAAT4 for glutamate is shown in Figure 2C (▲). The apparent ΔH^0 was determined to be -69 ± 5 kJ/mol, which is significantly higher than the one measured for EAAC1 (Table 1). ΔS^0 was also significantly more negative for EAAT4 with a value of -113 ± 5 J/K·mol, indicating enthalpy−entropy compensation for both EAAC1 and EAAT4.

The temperature dependence of the apparent K_m value for glutamate activation of transport current is determined by the temperature dependence of the intrinsic dissociation constant of glutamate from its transporter binding site, K_d, and additionally by kinetic factors (e.g., free energies of activation) of reactions preceding or following the glutamate binding step. To eliminate the influence of transport steps following substrate binding, we used a competitive inhibitor, DL-*threo*-β-benzyloxyaspartate (TBOA), which binds to the glutamate binding site, but is not transported by EAAC1 (*27*).

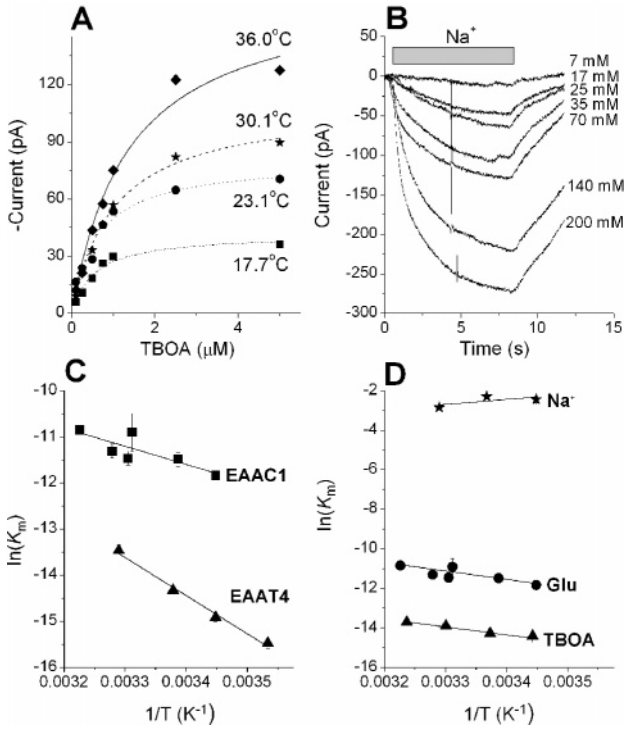

FIGURE 2: Binding of amino acid substrates, but not Na^+, is driven by a negative enthalpy change. (A) Original data showing the [TBOA] dependence of leak anion currents at temperatures of 17.7 °C (■), 23.1 °C (●), 30.1 °C (★), and 36 °C (♦). The pipet contained 140 mM KSCN. (B) Representative data from a single cell showing the $[Na^+]$ dependence of the leak anion conductance. Na^+ at concentrations ranging from 7 to 200 mM were applied to the transporter at the interval indicated by the bar. The pipet contained 140 mM KSCN. Non-transfected control cells responded to 200 mM Na^+ with an inward current of only -19 ± 2 pA. (C) van't Hoff plots of the apparent K_m for glutamate activation of the anion current for EAAC1 (■) and EAAT4 (▲). The lines represent linear regression analysis of the two data sets. (D) van't Hoff plots of the K_m of EAAC1 for TBOA (▲), and glutamate (●) and Na^+ (★). The K_m values were measured using the anion current as an assay (140 mM KSCN internal). The error bars indicate ±SEM. The transmembrane potential was 0 mV in all experiments.

Table 1: Summary of the Thermodynamic Parameters Derived for Glutamate Transport at Steady State and at 0 mV Transmembrane Potential

	ΔH^0 (kJ/mol)	ΔS^0 (J/K·mol)	ΔG^0 (kJ/mol)
EAAC1, apparent glutamate binding	-33 ± 6	-15 ± 8	-28 ± 1 (at 22.3 °C)
EAAT4, apparent glutamate binding	-69 ± 5	-113 ± 5	-35 ± 1 (at 23 °C)
EAAC1, Na^+-binding	$+15 \pm 16$		-7 ± 4 (at 24 °C)
EAAC1, TBOA-binding	-30 ± 3	$+16 \pm 4$	-35 ± 1 (at 23.5 °C)

TBOA inhibits the anion leak current of EAAC1 (*7*). We used this property to determine the temperature dependence of the K_m of EAAC1 for TBOA (Figures 2A and D). The K_m of EAAC1 for TBOA increased with increasing temperatures, about 2-fold in a 20 °C interval. From the resulting van't Hoff plot (Figure 2D, ▲) the apparent binding enthalpy of TBOA was determined to be $\Delta H^0 = -30 \pm 3$ kJ/mol. In contrast to apparent glutamate binding, which was associated with a negative entropy change, the apparent entropy change of the TBOA binding process was positive ($\Delta S^0 = +16 \pm 4$ J/K·mol). These results indicate that TBOA association with EAAC1 is exothermic and driven by both enthalpic and entropic components at room temperature.

Glutamate transport by EAAC1 is coupled to the cotransport of three sodium ions. At least one of the three cotransported Na^+ ions binds to the empty transporter, activating a leak anion current (Figure 2B and D, ★). The K_m of EAAC1 for sodium ions was determined from the Na^+ concentration dependence of this leak anion current. Within experimental error, this K_m did not change with temperature (Figure 2D). Thus, the reaction enthalpy for apparent Na^+ association with EAAC1 is not significantly different from zero ($\Delta H^0 = 15 \pm 16$ kJ/mol). These results suggest that Na^+ association with EAAC1 is driven by an increase in entropy. It should be noted that the K_m measurement for Na^+ is associated with a significantly larger error than the K_m measurements for glutamate because of the low affinity of EAAC1 for Na^+ ($K_m = 106 \pm 17$ mM at room temperature). Therefore, at a $[Na^+]$ of 200 mM, the maximum concentration used, the Na^+ binding site is far from being saturated. This large error of the K_m is reflected in the large uncertainty of the apparent ΔH^0.

Temperature Dependence of Glutamate Transporter Pre-Steady-State Kinetics. Transport current relaxations in response to submillisecond glutamate concentration jumps reflect early transitions in the EAAC1 transport cycle (*8*, *15*). As shown in Figure 3A and B, transport currents induced by submillisecond photolytic release of glutamate from 1 mM caged glutamate at room temperature (22 °C) consisted of a transient component and a steady-state current component. The decay of the transient transport current component was biphasic with a relaxation rate constant of the slowly decaying phase ($1/\tau_{slow}$(transport)) of 150 ± 5 s^{-1} at 0 mV transmembrane potential. $1/\tau_{slow}$ was strongly dependent on the transmembrane potential, increasing with hyperpolarization of the membrane (Figure 3C, ●). In contrast, the relaxation rate constant of the rapidly decaying phase ($1/\tau_{fast}$(transport) $= 1750 \pm 5$ s^{-1} at $V = 0$ mV) depended only weakly on the transmembrane potential and decreased with hyperpolarization of the membrane (Figure 3C, ○). These opposite voltage dependencies suggest that the two electrogenic components of the decay of the transport current are kinetically distinct and are not caused by the same underlying electrogenic transport process. The rise of the transient transport current after the glutamate concentration jump was not immediate. The current reached its maximum level at about 0.7 ms after the concentration jump (Figure 3B). The relaxation rate constant of this rising phase was $1/\tau_{rise}$(transport) $= 3000 \pm 500$ s^{-1} ($V = 0$ mV). This result suggests that a rapid, electroneutral (or weakly electrogenic) reaction precedes the electrogenic transport current.

To test whether the glutamate-induced transient transport current is caused by reactions of the glutamate-dependent transporter half-cycle or the K^+-dependent transporter half-cycle, we performed experiments analogous to the ones shown in Figure 3A while restricting the transporter to populate states associated with the glutamate translocation reaction (exchange mode). This was done by including glutamate and Na^+ into the recording electrode and excluding K^+, thus preventing EAAC1 from entering the K^+-dependent half-cycle. Rapid glutamate application to EAAC1 in the exchange mode induced a transient transport current (Figure 3D), which showed the same triphasic characteristics as those

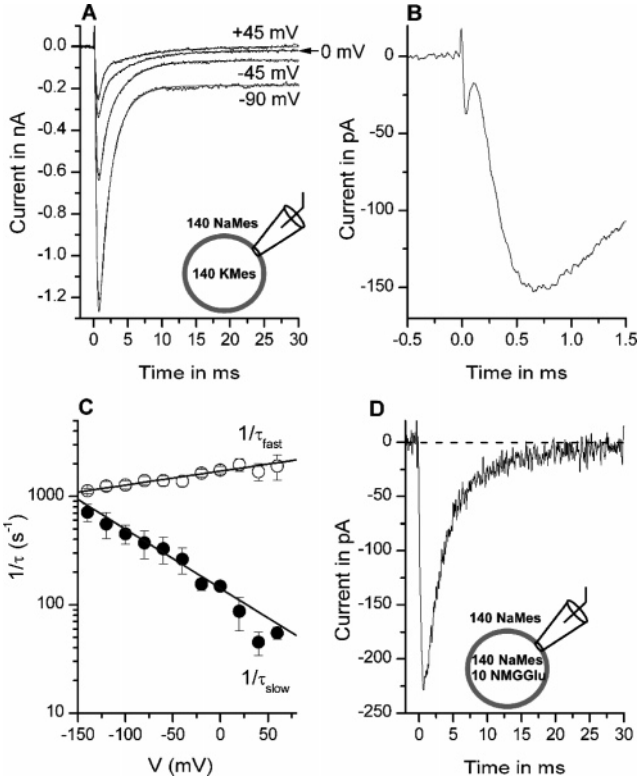

FIGURE 3: Glutamate-induced transport currents in EAAC1 consist of three kinetically distinct components. (A) Transport currents induced by photolytic release of glutamate from 1 mM caged glutamate at time $t = 0$ and at membrane potentials of +45, 0, −45, and −90 mV (from top to bottom trace). The pipet contained 140 mM KMes (forward transport conditions, see inset). The solid lines represent fits of a sum of three exponential terms and a steady-state current to the data. (B) Current trace recorded under conditions similar to those in (A) but shown with 20-fold higher magnification of the time axis to illustrate the rising phase of the current ($V = 0$ mV). (C) Relaxation rate constants ($1/\tau$) determined for the rapidly and slowly decaying phase of the glutamate-induced transport current as a function of the transmembrane potential. The pipet contained 140 mM KMes (forward transport conditions, see inset). (D) Transport current induced by the photolytic release of glutamate from 1 mM caged glutamate at time $t = 0$ and at a membrane potential of 0 mV. The pipet contained 140 mM NaMes and 10 mM glutamate (exchange conditions, see inset).

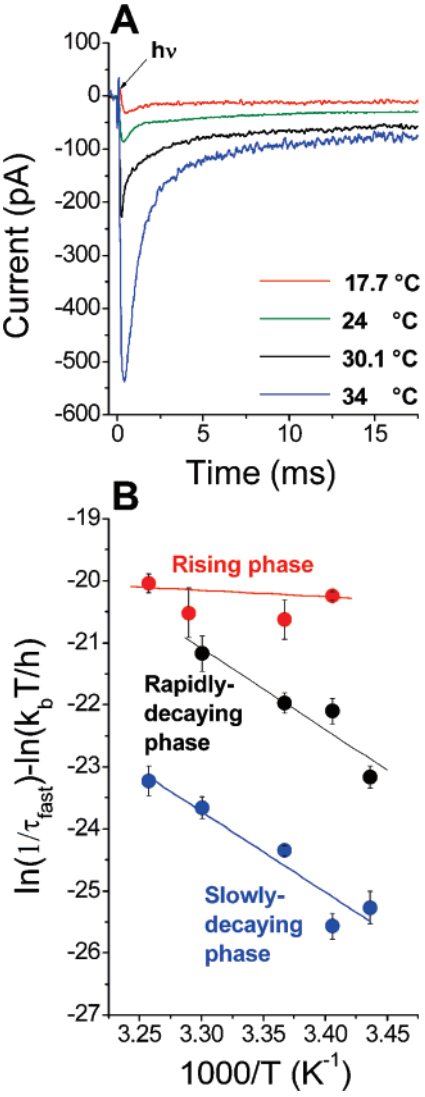

FIGURE 4: Two of the three phases of the glutamate-induced transport current are associated with a large activation barrier. (A) Original traces of glutamate-induced transport currents (KMes in the pipet) at different temperatures ranging from 17.7 to 34 °C, as indicated in the legend. Glutamate was photolytically released from the MNI-glutamate precursor (1 mM) at $t = 0$ ms, as indicated by the arrow. (B) Eyring plots of the apparent relaxation rate constants obtained from fitting data as shown in A to a sum of three exponentials (rising phase, red circles; rapidly decaying phase, black circles; slowly decaying phase, blue circels). The lines are the results of linear regression analyses. The transmembrane potential was 0 mV in all experiments.

of the current in the forward transport mode (Figure 3A) with similar relaxation rate constants, but the steady-state component of the current was absent. This similar nature of the transient current component in the forward transport mode and exchange mode suggests that the reaction steps responsible for the transient current follow glutamate binding from the extracellular side and precede glutamate and Na^+ dissociation to the cytoplasm (*15*). In the following paragraphs, we describe the temperature dependence of the relaxation rates of the three phases of the transient transport current to obtain a better understanding of the molecular nature of the underlying reaction steps of the transporter.

EAAC1 transport currents in response to a jump of the glutamate concentration at various temperatures ranging from 17.7 to 34 °C are shown in Figure 4A. Similar to the steady-state transport current, the peak of the transient current component showed strong temperature dependence with a Q_{10} value of 3.5 ± 2 ($n = 4$). The current response to glutamate application was triphasic with a rising phase and two decaying phases at 30 °C and lower temperatures. At 34 °C, the rising phase of the current was still observed, but the current decay consisted of only one phase (Figure 4A, blue trace). The relaxation rate constants associated with the three phases of the transient transport current increased with increasing temperature but with varying degrees. The relaxation rate $1/\tau_{rise}$(transport) showed only minor temperature dependence (Figure 4B, red circles), whereas $1/\tau_{fast}$(transport) was strongly temperature dependent. $1/\tau_{fast}$(transport) increased ~7.6-fold in a 12 °C temperature interval. At near physiological temperatures (~34 °C) this relaxation rate constant becomes very fast (0.08 ± 0.02 ms, $n = 4$, Figure 4A and B, black circles). In fact it becomes so fast that it cannot be resolved from the rising phase, which then becomes rate-limiting for the process associated with $1/\tau_{fast}$-(transport). The relaxation rate of the slowly decaying phase

Table 2: Activation Parameters Derived from Pre-Steady-State Transport Currents and Anion Currents (in Parenthesis) at 0 mV Transmembrane Potential

	$\Delta H^{\ddagger}$ (kJ/mol)	$\Delta S^{\ddagger}$ (J/K·mol)
$1/\tau_{rise}$	11 ± 10	
$1/\tau_{fast}$	121 ± 12 (116 ± 7 anion current)	222 ± 46 (206 ± 24 anion current)
$1/\tau_{slow}$	94 ± 5 (104 ± 20 anion current)	122 ± 15 (147 ± 66 anion current)

of the transient transport current is also strongly temperature dependent (Figure 4A and B, blue circles). To quantify and compare these data, we plotted the relaxation rates versus $1/T$ according to eq 4, as shown in Figure 4B. The data for all three phases were evaluated with a linear regression analysis because no deviations from linearity were observed, given the experimental errors. It is important to note that the activation parameters deduced from this analysis are apparent activation parameters because they were derived from observed relaxation rate constants and not intrinsic activation parameters of individual transporter reaction steps. The apparent activation enthalpy, $\Delta H^{\ddagger}$, for $1/\tau_{rise}$(transport) was determined to be 11 ± 10 kJ/mol (Figure 4B, Table 2). This low value of the activation enthalpy indicates that the rising phase of the transport current is rate-limited by a diffusion-controlled reaction. The apparent activation enthalpies for the two decaying phases of the current are listed in Table 2 and were much higher in the range of 100 kJ/mol. Because of such high values for the activation enthalpies, it appears unlikely that diffusional movement of ions within the protein causes the electrogenic charge movements associated with the two decaying phases of the transport current. Table 2 also shows the entropies of activation for the three phases of the transient transport current.

Since the apparent affinity of EAAC1 for glutamate changes within the 18 to 34 °C temperature range tested here, we have to consider the possibility that the observed relaxation rates increase with increasing temperature because the percent saturation of the glutamate binding site increases. This possibility can be excluded for two reasons: (1) The apparent affinity of EAAC1 decreases with increasing temperature (Figure 1A). Thus, the percent saturation of the glutamate binding site should be lower but not higher at increased temperature. (2) Although not precisely known, the photolytically released glutamate concentration should range from 150 to 200 μM (the percent photolytic glutamate release from 1 mM caged precursor is typically 15−20%, (*13*, *16*, *28*)), which is sufficient to saturate the EAAC1 glutamate binding site throughout the whole temperature range studied.

Next, we measured the temperature dependence of the glutamate-induced anion current. This was done under forward transport conditions, that is, 140 mM K^+ in the pipet solution and using intracellular SCN^- as the permeating anion. The photolytic release of glutamate from its caged precursor (1 mM) resulted in an inwardly directed anion current, which showed a rise to a maximum, followed by a decay to the steady-state current level (Figure 5A). The currents were fitted with a sum of two exponentials, which yielded the relaxation rate constants for the anion current rise, $1/\tau_{fast}$(anion), and the anion current decay, $1/\tau_{slow}$(anion). The amplitudes as well as the time constants associated with

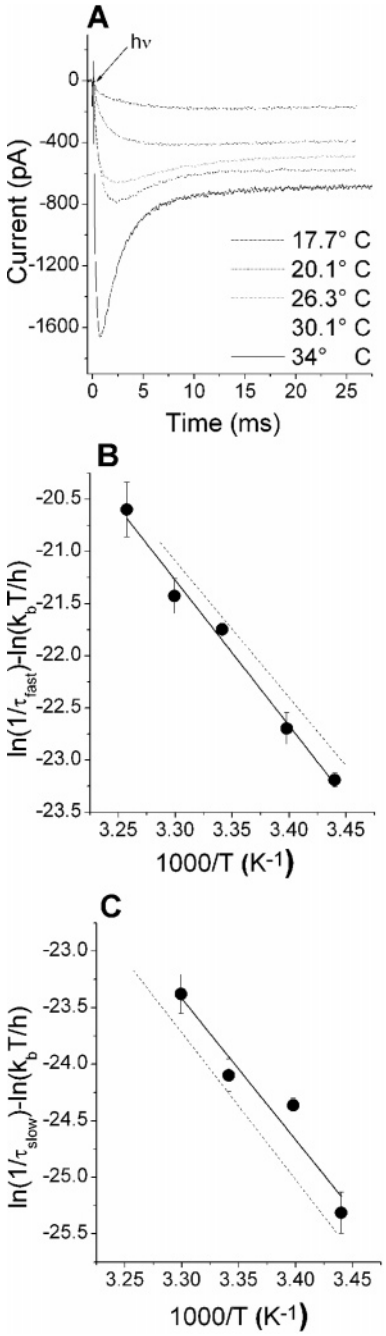

FIGURE 5: Time course of glutamate-induced anion currents reports on transitions in the transport cycle. (A) Original traces of glutamate-induced anion currents (KSCN in the pipet) at different temperatures ranging from 17.7 to 34 °C, as indicated in the legend. Glutamate was photolytically released from the MNI-glutamate precursor (1 mM) at $t = 0$ ms, as indicated by the arrow. (B and C) Eyring plots of the apparent relaxation rate constants obtained from fitting data as shown in A to a sum of two exponentials (rising phase, B; decaying phase, C) The lines are the results of linear regression analyses. The transmembrane potential was 0 mV in all experiments.

the two phases of the anion current were temperature-dependent. To quantify and compare these data, we plotted $\ln(1/\tau) - \ln(k_b T/h)$ obtained from the three phases of the transport current versus $1/T$ (eq 4), as shown in Figure 5B and C. The activation enthalpy for $1/\tau_{fast}$(anion) was $\Delta H^{\ddagger} = 119 \pm 7$ kJ/mol, and that of $1/\tau_{slow}$(anion) was $\Delta H^{\ddagger} = 104 \pm 20$ kJ/mol. These results suggest that partial reactions underlying both phases of the anion current are associated

with a large energy barrier. Table 2 summarizes the enthalpies and the entropy of activation for the two phases of the glutamate-induced anion current.

These data raise questions of whether there is a correlation between the microscopic kinetic processes associated with the two phases of the glutamate-induced anion current and two of the three phases of the transport current. It was proposed by Watzke and colleagues that the processes linked with $1/\tau_{fast}$(anion) reflect the same processes linked with $1/\tau_{fast}$(transport) (*15*). The time constants found here at 18 °C support this proposal (2.0 ± 0.4 ms for τ_{fast}(anion) vs 1.9 ± 0.3 ms for $1/\tau_{fast}$(transport)). The values for $\Delta H^{\ddagger}$ for $1/\tau_{fast}$(anion) and $1/\tau_{fast}$(transport) are identical within experimental error. The regression line calculated for $1/\tau_{fast}$(transport) is inserted into Figure 5B as a dashed line to illustrate this correlation. A similar correlation was also found for the absolute values and for the temperature dependencies of $1/\tau_{slow}$(anion) and $1/\tau_{slow}$(transport), as shown by the solid and the dashed lines in Figure 5C. These results suggest that the phases observed in the glutamate-induced anion current report on transitions in the EAAC1 transport cycle in the same way the phases associated with the glutamate-induced transport current do.

Finally, we determined the effect of the temperature on the transient currents induced by Na^+ binding to EAAC1 in the absence of transported substrate. In agreement with previous reports, step changes in the membrane potential from 0 mV to values ranging from −150 to +90 mV resulted in transient, TBOA-sensitive currents. These transient currents were capacitive in nature, as expected for the voltage-induced Na^+ binding and dissociation process, and decayed with a time constant of 0.76 ± 0.1 ms at 0 mV and 22 °C (Figure 6B). The charge, *Q*, moved in response to the voltage jump, which was obtained by integrating the transient current over time, started saturating at negative potentials, in agreement with previous results obtained for EAAT2 expressed in *Xenopus* oocytes (*29*). The voltage dependence of the charge movement could be quantitatively described using a Boltzmann relationship (eq 5 and Figure 6C). Although the midpoint potential of the charge movement, $V_{1/2}$, could not be determined accurately because of the lack of saturation at $V < +100$ mV, it can be estimated that $V_{1/2}$ is > +50 mV. This value agrees well with the theoretical $V_{1/2}$ (+57 mV) obtained from the previously determined K_m for Na^+ binding of 80−100 mM (eq 6). The rate of current relaxation after voltage jump was slightly voltage dependent (Figure 6D, circles) and increased at both negative and positive membrane potentials, as previously shown for EAAT2 (*29*). From fitting eq 7 to the experimental data, an apparent valence, z_Q, for the voltage-induced charge movement was determined to be 0.27. It should be noted that the EAAC1-specific relaxation rates obtained here are not limited by the rate constant of charging the membrane (Figure 6D, triangles), which was at least 3-times larger than the EAAC1-specific relaxation rates and was voltage-independent. Taken together, these data obtained at 22 °C agree well with previous results obtained by voltage-jump experiments in EAAC1 (*15*) and EAAT2 (*29*). After reducing the temperature to 18 °C, the decay of the transient currents was slowed only slightly (Figure 6A, C, and D), with Q_{10} values of 1.7 at −150 mV and 1.3 at +100 mV, respectively. These data suggest that the molecular process(es) underlying the decay

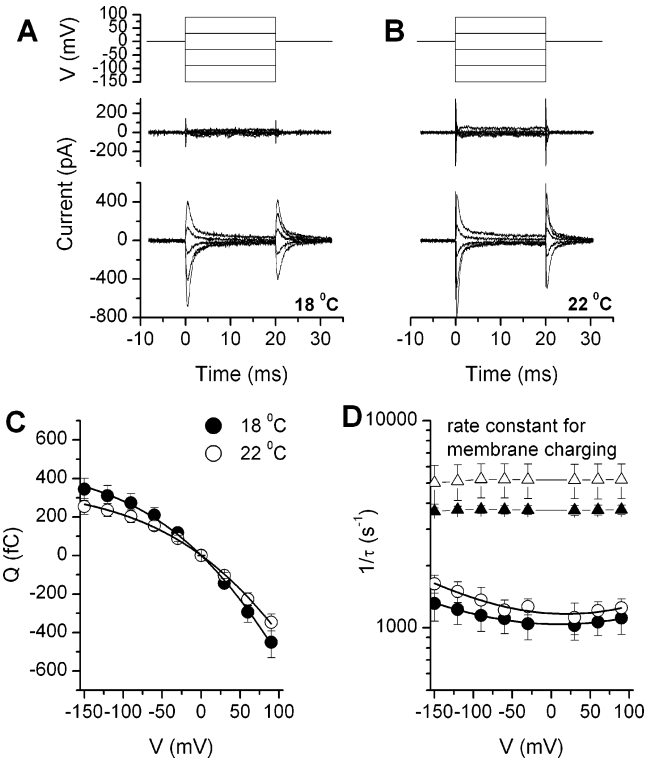

FIGURE 6: Transient currents caused by Na^+ binding to EAAC1 are only weakly temperature dependent. Transient currents induced by applying step changes in the transmembrane potential (the voltage protocol is shown in the top panel) to the EAAC1 expressing Cos-7 cells at 18 °C (A) and 22 °C (B). Experiments were performed in exchange mode, with 140 mM Na^+ and 10 mM glutamate in the pipet. EAAC1-specific currents were obtained by subtraction of currents in the presence of TBOA from those in the absence of TBOA (lower panel) and in the presence of 140 mM extracellular Na^+, as described previously (*15*, *29*). The middle panel shows control traces obtained by subtracting currents from two runs before and after TBOA application, showing that the electrical characteristics of the cell membrane are unchanged throughout the course of the sequence of experiments. (C) Voltage dependence of the charge movement in response to voltage jumps at 18 °C (●) and at 22 °C (○) obtained by integrating the currents. (D) Voltage dependence of relaxation rate constant of voltage jump-induced current decay at 18 °C (●) and at 22 °C (○). The triangles represent the rate constant for charging of the cell membrane at 18 °C (▲) and at 22 °C (△).

of the transient current is/are almost temperature independent. At −150 mV, the apparent relaxation rate constant is expected to be dominated by the rate constant of Na^+ binding (k_f in eq 7), whereas at +100 mV, the rate of Na^+ dissociation should dominate this rate (k_b in eq 7). Therefore, our data suggest that both Na^+ binding and dissociation steps are low-barrier, diffusion-limited processes.

DISCUSSION

Here, we investigated the effects of temperature on the steady-state and pre-steady-state kinetics of glutamate transport by EAAC1. Our data demonstrate that the apparent dissociation constant, K_m, of EAAC1 for glutamate increases with increasing temperature (Figure 2A). This result suggests that glutamate binding to EAAC1 is exothermic and, at room temperature, driven by negative reaction enthalpy ($\Delta H^0 = -33$ kJ/mol). At 22 °C, the entropic component does not contribute significantly to this glutamate binding process (Table 1). Because we measured the apparent affinity of

EAAC1 for glutamate, the thermodynamic parameters determined here are apparent parameters because reaction steps preceding or following glutamate binding in the transport cycle contribute to this apparent affinity. Furthermore, forward transport of glutamate is a nonequilibrium process. Interpretations of results from nonequilibrium processes by using equilibrium thermodynamic approaches have to be viewed with caution. To obtain an understanding of how other temperature-dependent reactions in the transport cycle affect the temperature dependence of the apparent K_m for glutamate, we calculated the expected ΔH^0 for the limiting case that glutamate binding itself is not temperature dependent. We used the following simplified kinetic scheme, which includes the temperature-dependent reaction steps identified below.

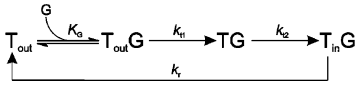

According to this scheme, the apparent K_m for glutamate at steady state can be expressed as follows:

$$K_m = K_G \frac{k_{t2}k_r}{k_{t2}k_r + k_{t1}(k_{t2} + k_r)} \quad (8)$$

Here, k_{t1} and k_{t2} are the rate constants of the fast and slow steps associated with translocation, respectively, and k_r is the rate constant for transporter relocation. If K_G, the intrinsic dissociation constant of glutamate from EAAC1, is assumed to be temperature independent, we calculate a ΔH^0 of +44 kJ/mol for the apparent K_m of glutamate. The sign of this value is opposite that of the experimentally determined apparent ΔH^0, suggesting that the real ΔH^0 for glutamate binding is even more negative than −33 kJ/mol. Therefore, we propose that glutamate association with its binding site on EAAC1 is driven by a large heat release, suggesting that more hydrogen bonds may be formed upon binding of glutamate to EAAC1 than are destroyed upon de-solvation of glutamate. Alternatively, the number of hydrogen bonds may stay the same, but stronger bonds are formed, or the number of hydrogen bonds may increase, and stronger hydrogen bonds are formed.

To further test this idea, we determined the effect of temperature on the interaction of TBOA with its binding site on EAAC1. TBOA is a non-transportable, competitive inhibitor of glutamate transporters, which is thought to bind to the glutamate binding site. When TBOA is bound to EAAC1, the transporter cannot change its structure to expose the substrate binding site to the cytoplasm. Thus, the interaction of TBOA with EAAC1 is an equilibrium process. Therefore, thermodynamic parameters determined from TBOA interaction with EAAC1 should not be affected by the problems of interpretation noted above for glutamate as a substrate. The van't Hoff plots of the K_m of EAAC1 for TBOA (Figure 2D) revealed an apparent binding enthalpy of −30.0 kJ/mol, suggesting that the binding of TBOA to EAAC1 is exothermic. Within experimental error, this value of ΔH^0 is identical to the one measured for the glutamate effect on EAAC1.

The apparent substrate-binding enthalpies determined here for EAAC1 can be compared to the ones found in other glutamate binding proteins, as determined by calorimetry. For example, glutamine synthase binds glutamate with a $\Delta H^0 = -24$ kJ/mol (*30*). Of special interest is glutamate binding to the glutamate binding domain of glutamate receptors (S1S2-domain), a process that has been characterized well. In contrast to EAAC1, the glutamate binding enthalpy of this S1S2-domain is dependent on temperature. Therefore, we compared the parameters reported here for EAAC1 with the parameters reported for the S1S2-domain at 25 °C. Interestingly, in both proteins a conserved arginine residue is involved in the binding of a carboxy function of the substrate, but in S1S2-domain, arginine 485 binds the α-carboxy group (*31*), whereas in EAAC1, the γ-carboxy group associates with arginine 447 (*32*). In both cases, the binding enthaply is negative, and it can be speculated that the enthalpy derived from ion pair formation contributes to the heat released upon substrate binding. However, the geometry of both binding pockets is too different to draw further detailed conclusions.

In contrast to the dose-dependence of activation of the EAAC1 transport current by glutamate, which is associated with a small decrease of the apparent entropy, TBOA binding to EAAC1 results in an entropy increase of about 16 J/K·mol. This entropy increase is mainly responsible for the high affinity of EAAC1 for TBOA as compared to glutamate. The entropy increase could be due to the release of bound water molecules. Because TBOA has a hydrophobic benzyl group, which probably interacts with a hydrophobic surface in the EAAC1 substrate binding pocket, the release of structured water molecules from the binding pocket upon TBOA binding could explain this entropy increase. Thus, the hydrophobic effect appears to be the main reason why TBOA interacts strongly with EAAC1.

It was shown previously that the glutamate transporter subtype EAAT4 binds glutamate with about 10-fold higher apparent affinity than the subtype EAAT3 (*13*, *33*). Here, we found that the negative apparent glutamate binding enthalpy of EAAT4 is about twice as large as that of EAAC1. Therefore, the higher apparent affinity of EAAT4 for glutamate is, at least in part, caused by the stronger molecular interaction of glutamate with its binding site on EAAT4 (stronger hydrogen bonding). This could indicate a different substrate-binding environment in these two glutamate transporter subtypes. However, this more negative enthalpy of EAAT4 is offset partly by a more negative binding entropy, resulting in entropy−enthalpy compensation.

In addition to examining the effects of temperature on the apparent affinities of EAAC1 for substrates, we obtained activation parameters for the kinetics of rapid processes in the EAAC1 transport cycle. The glutamate-induced transport current shows a large, rapidly decaying transient component, which consists of three phases: a rising phase, a rapidly decaying phase, and a slowly decaying phase (Figure 3A). Temperature had a weak effect on the rising phase but a strong effect on the two decaying phases. Before interpreting these data, it should be noted that these activation parameters are apparent parameters, which reflect the effect of temperature on the eigenvalues of the system and not on the individual reactions in the transport cycle. Nevertheless, by restricting the transporter to populate specific states in this cycle, it is possible to draw conclusions about the activation parameters of individual reaction steps. To this extent, we

have restricted EAAC1 to the translocation branch of the transport cycle by saturating the intracellular binding sites for Na^+ and glutamate (exchange mode). These ionic conditions prevent intracellular dissociation of Na^+ and glutamate and inhibit the completion of the transport cycle through the K^+-dependent branch of the cycle. The three phases observed for the glutamate-induced transport current in the forward transport mode were also present in the exchange mode (Figure 3D), indicating that they are caused by glutamate and/or sodium association with EAAC1, and/or translocation of the substrates across the membrane. We assigned the rising phase of the transport current to the glutamate binding reaction. We estimated a bimolecular rate constant for glutamate binding of $2 \times 10^7\ M^{-1}\ s^{-1}$, consistent with a value we determined earlier from measuring the rate of the anion current rise at low glutamate concentrations (*7*). The activation enthalpy of the rate of the rise in transport current is 11 kJ/mol, indicating that this process is not associated with a conformational change. Activation enthalpies of diffusion-controlled reactions in water are typically in the 10−20 kJ/mol range (*25*). This low activation enthalpy supports our assignment of the current rising phase to the glutamate binding process, which is most likely diffusion-controlled. Our data suggest that Na^+ binding from the extracellular side is also a diffusion-controlled process because charge movement from Na^+ moving into its binding site is associated with low activation energy (Q_{10} of 1.7). This result is in agreement with data reported for the GABA transporter (*34*), which also shows a low-barrier Na^+ binding process.

In contrast to the low barrier associated with the transport current rising phase, the relaxation rate constants for the two decaying phases show high activation enthalpies, both in the range of 110 kJ/mol. These values are not consistent with diffusional processes but indicate that conformational changes underlie these two phases of the transport current, as proposed previously by us (*7*, *15*). Because the activation enthalpies associated with the rapidly and slowly decaying phases of the transient transport current have similar values, the possibility has to be considered that these two phases are not caused by independent electrogenic processes but that one, strongly temperature-dependent process determines the rate of both phases. However, this possibility can be rejected because the relaxation rate constants of the two phases are differentially affected by the transmembrane potential (Figure 3B). Whereas $1/\tau_{slow}$(transport) increases at hyperpolarized potentials, $1/\tau_{fast}$(transport) decreases. Thus, both phases must be rate limited by reactions that have opposite voltage dependence and cannot be caused by the same process. This interpretation is consistent with previous data showing that both decaying phases of the transient transport current are also differentially affected by extracellular Na^+ concentration (*15*).

On the basis of the results of our experiments and the crystal structure of the bacterial aspartate transporter GltPh (*12*, *35*), we propose a modified transport model, as illustrated in Figure 7. As proposed by Yernool et al. (*12*), our model includes an extracellular gate (re-entrant loop 2, RL2) and an intracellular gate (re-entrant loop 1, RL1), which can open one at a time to allow access of glutamate to its binding site either from the extracellular or from the intracellular side of the membrane. In the first step, diffusion-controlled Na^+ binding to EAAC1 reorganizes the transporter and creates a high affinity glutamate binding site. (Na^+ binding steps are not shown in Figure 7 for simplicity.) Exothermic glutamate binding following this Na^+ binding step is diffusion-controlled (low $\Delta H^{\ddagger}$), suggesting the existence of a water-filled extracellular access pathway to the glutamate binding site when the extracellular gate is open. The binding of glutamate leads to a conformational change, which we interpret as the transition to an occluded state (Figure 7) brought about by closure of the extracellular gate (*35*). We suggest that the closure of the extracellular gate is electrically manifested as the rapidly decaying phase of the transport current. The occluded state is conducting anions. The significant activation entropy associated with this occlusion reaction implies the release of water molecules from nonpolar surfaces of the protein during this transition. The following step, which is associated with $1/\tau_{slow}$(transport), was previously interpreted by us and by others as the glutamate translocation reaction (*7*, *8*, *15*). In comparison to Yernool et al. (*12*), this translocation reaction can alternatively be interpreted as opening the intracellular gate, which is expected to be associated with high activation energy. Taken together, our findings support the proposed alternating access model (*12*, *36*). Our results imply that at least two conformational changes are associated with glutamate

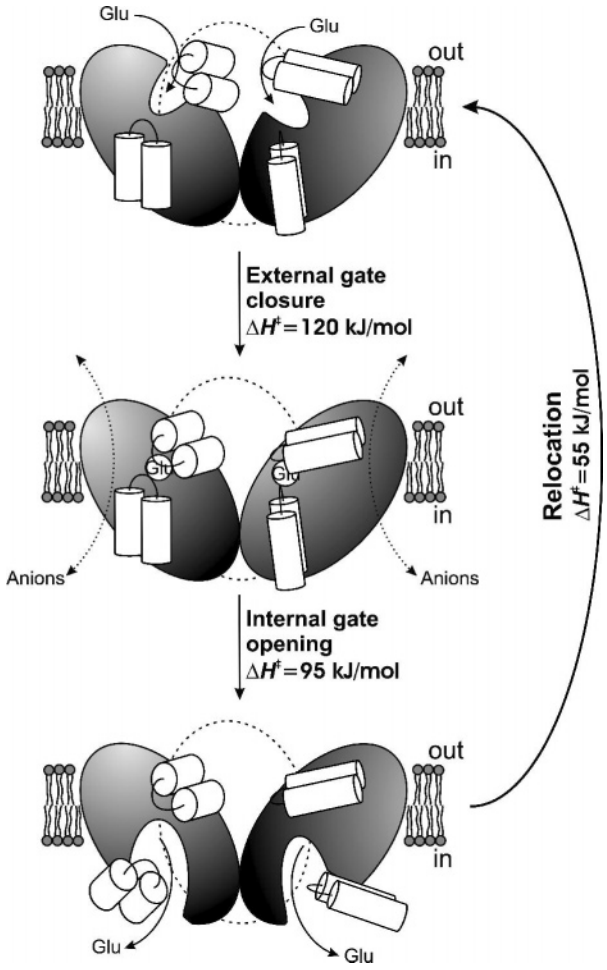

FIGURE 7: Hypothetical mechanism of glutamate transport by EAAC1, in analogy to the structural model proposed by Yernool and colleagues for GltPh (*12*). Two of the three subunits in the trimeric assembly are shown in the side view. The third subunit is indicated by the dashed line.

translocation and that rates of these conformational changes have opposite dependence on the transmembrane potential. The existence of such conformational changes is consistent with a variety of data from biochemical studies and fluorescence measurements (*37*−*41*).

Our data also show that steady-state glutamate transport by EAAC1 is associated with high activation energy, consistent with an earlier report on EAAT2 (*9*) and glutamate transporters in Purkinje cells (*1*). It was proposed previously by us and others that at room temperature the steady-state rate of glutamate transport is mainly limited by the K^+-dependent relocation of the transporter (*7*, *8*, *42*). Therefore, it is likely that steps in this relocation process also involve conformational changes. It can be speculated that this relocation process involves a reversal of the gate opening/closing transitions shown in Figure 7 for the translocation process. Although the model shown in Figure 7 is attractive because of its symmetry with respect to the plane of the membrane, it should be noted that unlike in another secondary active transporter of known structure (*43*, *44*), the proposed binding site for the substrate in GltPh is not localized in the center of the membrane (Figure 7) but localized rather close to the extracellular face of the protein (*35*). This could imply that glutamate dissociation into the cytoplasm is not diffusion-controlled because glutamate leaves its binding site through an access channel. Future experimentation will be necessary to test this hypothesis.

Finally, we investigated the temperature dependence of EAAC1-associated anion currents carried by SCN^-. These anion currents were previously shown to be a sum of two different current components, a glutamate-dependent anion current and a leak anion current. The glutamate-induced anion current at steady state shows a relatively weak temperature dependence ($Q_{10} = 1.9 \pm 0.4$, $n = 4$). This result is consistent with previous data on transporter generated anion currents in Purkinje cells ($Q_{10} = 1.07 \pm 0.18$) (*1*) and recombinantely expressed transporters (*9*), implying only minor rearrangements of the protein to maintain anion conductivity.

We also evaluated the temperature dependence of the kinetics of the glutamate-induced anion currents after the rapid application of glutamate. The pre-steady-state anion current is composed of a rising phase and a decaying phase. It was proposed previously that these two phases of the anion current report on transitions in the transport cycle that are also observed in the pre-steady-state transport current, with the rising phase of the anion current being equivalent to the rapidly decaying phase of the anion current and the decaying phase of the anion current being equivalent to the slowly decaying phase of the transport current (*15*). Consistent with this proposal, the relaxation rate constants of both phases of the anion current are strongly temperature-dependent and show activation parameters that are similar to the ones observed for the two decaying phases of the transient transport current (Figure 5). These findings support previous conclusions that the glutamate-induced anion current can be used as a reliable reporter of transitions in the EAAC1 transport cycle (*15*, *16*, *28*).

The data reported here may be important to understand the contribution of glutamate transporters to glutamate removal from the synapse. Grewer et al. reported previously that glutamate translocation by EAAC1 takes place with a rate constant of about 400 s^{-1} at physiological transmembrane potentials (−90 mV) and at room temperature (*7*). Data from this work suggest that the rate of the slow process associated with glutamate translocation is about 8-fold higher at physiological temperatures compared to that at room temperature (at 0 mV). Consequently, it can be extrapolated that glutamate translocation will take place with a rate of about 3000 s^{-1} at 37 °C and at −90 mV. Although the contribution of EAAC1 to the removal of synaptically released glutamate may be minor (*45*), it is likely that the astrocytic transporters EAAT1 and EAAT2 transport glutamate on the basis of similar conformational changes of the protein with high activation barriers of the translocation-associated reactions. Therefore, it can be speculated that the removal of released glutamate can be rapid through the translocation process occurring within 300 μs, whereas recycling of the glutamate binding sites of the transporter takes place with a time constant of about 2 to 3 ms at physiological temperatures.

ACKNOWLEDGMENT

We thank Dr. T. Rauen for the pBK-CMVΔ expression plasmid.

REFERENCES

1. Auger, C., and Attwell, D. (2000) Fast removal of synaptic glutamate by postsynaptic transporters, *Neuron 28*, 547−558.
2. Brasnjo, G., and Otis, T. S. (2001) Neuronal glutamate transporters control activation of postsynaptic metabotropic glutamate receptors and influence cerebellar long-term depression, *Neuron 31*, 607−616.
3. Gaal, L., Roska, B., Picaud, S. A., Wu, S. M., Marc, R., and Werblin, F. S. (1998) Postsynaptic response kinetics are controlled by a glutamate transporter at cone photoreceptors, *J. Neurophysiol. 79*, 190−196.
4. Overstreet, L. S., Kinney, G. A., Liu, Y. B., Billups, D., and Slater, N. T. (1999) Glutamate transporters contribute to the time course of synaptic transmission in cerebellar granule cells, *J. Neurosci. 19*, 9663−9673.
5. Takayasu, Y., Iino, M., and Ozawa, S. (2004) Roles of glutamate transporters in shaping excitatory synaptic currents in cerebellar Purkinje cells, *Eur. J. Neurosci. 19*, 1285−1295.
6. Diamond, J. S., and Jahr, C. E. (1997) Transporters buffer synaptically released glutamate on a submillisecond time scale, *J. Neurosci. 17*, 4672−4687.
7. Grewer, C., Watzke, N., Wiessner, M., and Rauen, T. (2000) Glutamate translocation of the neuronal glutamate transporter EAAC1 occurs within milliseconds, *Proc. Natl. Acad. Sci. U.S.A. 97*, 9706−9711.
8. Otis, T. S., and Kavanaugh, M. P. (2000) Isolation of current components and partial reaction cycles in the glial glutamate transporter EAAT2, *J. Neurosci. 20*, 2749−2757.
9. Wadiche, J. I., and Kavanaugh, M. P. (1998) Macroscopic and microscopic properties of a cloned glutamate transporter/chloride channel, *J. Neurosci. 18*, 7650−7661.
10. Kanner, B. I., and Bendahan, A. (1982) Binding order of substrates to the sodium and potassium ion coupled L-glutamic acid transporter from rat brain, *Biochemistry 21*, 6327−6330.
11. Rodriguez, B. M., Sigg, D., and Bezanilla, F. (1998) Voltage gating of Shaker K+ channels. The effect of temperature on ionic and gating currents, *J. Gen. Physiol. 112*, 223−242.
12. Yernool, D., Boudker, O., Jin, Y., and Gouaux, E. (2004) Structure of a glutamate transporter homologue from *Pyrococcus horikoshii*, *Nature 431*, 811−818.
13. Mim, C., Balani, P., Rauen, T., and Grewer, C. (2005) The glutamate transporter subtypes EAAT4 and EAATs 1−3 transport glutamate with dramatically different kinetics and voltage dependence but share a common uptake mechanism, *J. Gen. Physiol. 126*, 571−589.
14. Hamill, O. P., Marty, A., Neher, E., Sakmann, B., and Sigworth, F. J. (1981) Improved patch-clamp techniques for high-resolution

current recording from cells and cell-free membrane patches, *Pflug. Arch. 391*, 85−100.
15. Watzke, N., Bamberg, E., and Grewer, C. (2001) Early intermediates in the transport cycle of the neuronal excitatory amino acid carrier EAAC1, *J. Gen. Physiol. 117*, 547−562.
16. Tao, Z., Zhang, Z., and Grewer, C. (2006) Neutralization of the aspartic acid residue Asp-367, but not Asp-454, inhibits binding of Na+ to the glutamate-free form and cycling of the glutamate transporter EAAC1, *J. Biol. Chem. 281*, 10263−10272.
17. Grewer, C. (1999) Investigation of the alpha(1)-glycine receptor channel-opening kinetics in the submillisecond time domain, *Biophys. J. 77*, 727−738.
18. Canepari, M., Nelson, L., Papageorgiou, G., Corrie, J. E. T., and Ogden, D. (2001) Photochemical and pharmacological evaluation of 7-nitroindolinyl-and 4-methoxy-7-nitroindolinyl-amino acids as novel, fast caged neurotransmitters, *J. Neurosci. Methods 112*, 29−42.
19. Connors, K. A. (1990) *Chemical Kinetics*, Wiley-VCH, New york.
20. Tommila, E., and Hinshelwood, C. N. (1938) The activation energy of organic reactions. Part IV. Transmission of substituent influences in ester hydrolysis, *J. Chem. Soc.*, 1801−1810.
21. Barabas, K., and Keszthelyi, L. (1984) Temperature dependence of ATP release from "caged" ATP, *Acta Biochim. Biophys. Acad. Sci. Hung. 19*, 305−309.
22. van't Hoff, J. H. (1884) *Etudes de Dynamique Chimique*, F. Muller, Amsterdam.
23. Eyring, H. (1935) The activated complex in chemical reactions, *J. Chem. Phys.*, 107−115.
24. Watzke, N., and Grewer, C. (2001) The anion conductance of the glutamate transporter EAAC1 depends on the direction of glutamate transport, *FEBS Lett. 503*, 121−125.
25. Stein, W. D. (1967) *The Movement of Molecules across Cell Membranes*, Academic Press, New York.
26. Otis, T. S., and Jahr, C. E. (1998) Anion currents and predicted glutamate flux through a neuronal glutamate transporter, *J. Neurosci. 18*, 7099−7110.
27. Shimamoto, K., Lebrun, B., Yasuda-Kamatani, Y., Sakaitani, M., Shigeri, Y., Yumoto, N., and Nakajima, T. (1998) DL-threo-beta -benzyloxyaspartate, a potent blocker of excitatory amino acid transporters, *Mol. Pharmacol. 53*, 195−201.
28. Tao, Z., and Grewer, C. (2005) The conserved histidine 295 does not contribute to proton cotransport by the glutamate transporter EAAC1, *Biochemistry 44*, 3466−3476.
29. Wadiche, J. I., Arriza, J. L., Amara, S. G., and Kavanaugh, M. P. (1995) Kinetics of a human glutamate transporter, *Neuron 14*, 1019−1027.
30. Ginsburg, A., Gorman, E. G., Neece, S. H., and Blackburn, M. B. (1987) Thermodynamics of active-site ligand binding to *Escherichia coli* glutamine synthetase, *Biochemistry 26*, 5989−5996.
31. Kasper, C., Pickering, D. S., Mirza, O., Olsen, L., Kristensen, A. S., Greenwood, J. R., Liljefors, T., Schousboe, A., Watjen, F., Gajhede, M., Sigurskjold, B. W., and Kastrup, J. S. (2006) The structure of a mixed GluR2 ligand-binding core dimer in complex with (S)-glutamate and the antagonist (S)-NS1209, *J. Mol. Biol. 357*, 1184−1201.
32. Bendahan, A., Armon, A., Madani, N., Kavanaugh, M. P., and Kanner, B. I. (2000) Arginine 447 plays a pivotal role in substrate interactions in a neuronal glutamate transporter, *J. Biol. Chem. 275*, 37436−37442.
33. Fairman, W. A., Vandenberg, R. J., Arriza, J. L., Kavanaugh, M. P., and Amara, S. G. (1995) An excitatory amino-acid transporter with properties of a ligand-gated chloride channel, *Nature 375*, 599−603.
34. Binda, F., Bossi, E., Giovannardi, S., Forlani, G., and Peres, A. (2002) Temperature effects on the presteady-state and transport-associated currents of GABA cotransporter rGAT1, *FEBS Lett. 512*, 303−307.
35. Boudker, O., Ryan, R. M., Yernool, D., Shimamoto, K., and Gouaux, E. (2007) Coupling substrate and ion binding to extracellular gate of a sodium-dependent aspartate transporter, *Nature 445*, 387−393.
36. Jardetzky, O. (1966) Simple allosteric model for membrane pumps, *Nature 211*, 969−970.
37. Grunewald, M., and Kanner, B. (1995) Conformational changes monitored on the glutamate transporter GLT-1 indicate the existence of two neurotransmitter-bound states, *J. Biol. Chem. 270*, 17017−17024.
38. Grunewald, M., and Kanner, B. I. (2000) The accessibility of a novel reentrant loop of the glutamate transporter GLT-1 is restricted by its substrate, *J. Biol. Chem. 275*, 9684−9689.
39. Larsson, H. P., Tzingounis, A. V., Koch, H. P., and Kavanaugh, M. P. (2004) Fluorometric measurements of conformational changes in glutamate transporters, *Proc. Natl. Acad. Sci. U.S.A. 101*, 3951−3956.
40. Ryan, R. M., and Vandenberg, R. J. (2002) Distinct conformational states mediate the transport and anion channel properties of the glutamate transporter EAAT-1, *J. Biol. Chem. 277*, 13494−13500.
41. Leighton, B. H., Seal, R. P., Watts, S. D., Skyba, M. O., and Amara, S. G. (2006) Structural rearrangements at the translocation pore of the human glutamate transporter, EAAT1, *J. Biol. Chem. 281*, 29788−29796.
42. Bergles, D. E., Tzingounis, A. V., and Jahr, C. E. (2002) Comparison of coupled and uncoupled currents during glutamate uptake by GLT-1 transporters, *J. Neurosci. 22*, 10153−10162.
43. Abramson, J., Smirnova, I., Kasho, V., Verner, G., Kaback, H. R., and Iwata, S. (2003) Structure and mechanism of the lactose permease of *Escherichia coli*, *Science 301*, 610−615.
44. Yamashita, A., Singh, S. K., Kawate, T., Jin, Y., and Gouaux, E. (2005) Crystal structure of a bacterial homologue of Na+/Cl− dependent neurotransmitter transporters, *Nature 437*, 215−223.
45. Nieoullon, A., Canolle, B., Masmejean, F., Guillet, B., Pisano, P., and Lortet, S. (2006) The neuronal excitatory amino acid transporter EAAC1/EAAT3: does it represent a major actor at the brain excitatory synapse? *J. Neurochem. 98*, 1007−1018.

BI7005465